

Theoretical investigation on the soft X-ray spectrum of the highly-charged W^{54+} ions

Xiaobin Ding^{a,*}, Jiaoxia Yang^a, Fumihiro Koike^b, Izumi Murakami^c, Daiji Kato^c, Hiroyuki A Sakaue^c, Nobuyuki Nakamura^d, Chenzhong Dong^a

^a*Key Laboratory of Atomic and Molecular Physics and Functional Materials of Gansu Province, College of Physics and Electronic Engineering, Northwest Normal University, Lanzhou 730070, China*

^b*Department of physics, Sophia University, Tokyo 102-8554, Japan*

^c*National Institute for Fusion Science, Toki, Gifu 509-5292, Japan*

^d*Institute for Laser Science, The University of Electro-Communications, Chofu, Tokyo 182-8585, Japan*

Abstract

A detailed level collisional-radiative model of the E1 transition spectrum of Ca-like W^{54+} ion has been constructed. All the necessary atomic data has been calculated by relativistic configuration interaction (RCI) method with the implementation of Flexible Atomic Code (FAC). The results are in reasonable agreement with the available experimental and previous theoretical data. The synthetic spectrum has explained the EBIT spectrum in 29.5-32.5 Å, while several new strong transitions has been proposed to be observed in 18.5-19.6 Å for the future EBIT experiment with electron density $n_e = 10^{12} \text{ cm}^{-3}$ and electron beam energy $E_e = 18.2 \text{ keV}$.

Keywords: Collisional-radiative model, Ca-like Tungsten, Relativistic configuration interaction

1. Introduction

Tungsten (W) and its alloy had been used as the armor plate material for the plasma facing component in the divertor region of ITER (International Thermonuclear Experimental Reactor Tokamak) and the other magnetic confinement

*Corresponding author.

Email address: dingxb@nwnu.edu.cn (Xiaobin Ding)

fusion reactors because of their high melting point, low sputtering yield, and low tritium retention rate[1, 2]. However, tungsten impurity ions might be produced during the plasma-wall interaction in the edge and then they might be transported to the high-temperature core plasma region. In the core plasma, these tungsten impurities can be ionized further to highly charged ions and radiate high energy photons. Therefore, the large radiation loss can be caused by these highly charged tungsten impurity ions, which will lead to the plasma disruption if the relative concentration of W ions in the core plasma is higher than about 10^{-5} [3]. Monitoring and controlling the flux of the highly charged W impurity ions are crucial to the success of the fusion[4]. Thus a thorough knowledge of the atomic properties of tungsten ions were strongly needed by the magnetic confinement fusion research. Furthermore, the spectra of tungsten impurity ions observed from the fusion plasma also provide plenty of important information about the fusion plasma parameters such as electron density, electron temperature, and ion temperature. Therefore, it can also be used to diagnose the plasma.

There are many research works related to the energy levels and transition properties of tungsten in various ionization stage in the past several decades[5–10], where only a few studies have focused on W^{54+} ion[11–17]. Y. Ralchenko *et al.* used the electron beam ion trap (EBIT) to observe the M1 spectrum from $3d^n$ ($n=1-9$) ground state fine structure multiplets of Co-like W^{47+} to K-like W^{55+} ions and a non-Maxwellian collisional-radiative model (CRM) was used to analyze the observed spectrum[17]. U. I. Safronova and A. S. Safronova calculated the wavelength and transition rates of the magnetic dipole (M1) and electric quadrupole (E2) transitions between the multiplets of the ground state configuration ($[Ne]3s^23p^63d^2$) of W^{54+} ion by using relativistic many-body perturbation theory (RMBPT)[15]. P. Quinet used a full relativistic Dirac-Fock method to calculate the line wavelengths and transition rates of the forbidden transitions within the $3p^k$ ($k=1-5$) and $3d^n$ ($n=1-9$) ground state configuration multiplets from Al-like W^{61+} to Co-like W^{47+} ions[16]. Dipti *et al.* calculated the excitation energies and the electron collisional excitation cross sections of

Ca-like W^{54+} ion by relativistic distorted wave theory[12]. C. F. Fischer *et al.* found the core correlation is very important for the transition energies of $3d^k$ configuration in tungsten ions[18].

T. Lennartsson *et al.* observed the electric dipole (E1) transitions from the excited states $[Ne]3s^23p^53d^3$ to the ground state $[Ne]3s^23p^63d^2$ of W^{54+} ion in the wavelength range of 26.3-43.5Å in the Lawrence Livermore National Laboratory (LLNL) EBIT at the electron beam energy of 18.2 keV, and a CRM was applied to explain the observed spectrum[13]. Ding and his collaborators have performed a calculation on the E1, E2, M1, M2 transitions between $[Ne]3s^23p^53d^3$ and $[Ne]3s^23p^63d^2$ levels of W^{54+} ion by using an MCDF method with the restricted active space method; the relativistic and electron correlation effects as well as the Breit interaction and some Quantum Electrodynamics effects have been taken into account[11, 19, 20]. The results are in reasonable agreement with available experimental data for both M1 and E1 transition lines. Several strong E1 transitions have been predicted. Some of these strong transitions are in good agreement with the observation from the EBIT, while others were not observed even in the similar wavelength range with similar transition rates. And some transitions with wavelength in 18.5-19.6 Å are suggested to be observed in the future experiment.

The present paper focuses on the explanation of the E1 transition spectrum of W^{54+} ion from the EBIT with the electron density $n_e = 10^{12} \text{ cm}^{-3}$ and the energy of electron beam $E_e = 18.2 \text{ keV}$ by CRM. The present paper is constructed as follows. In section 2, the theory of CRM and the calculation of the necessary atomic data are described. The result of the present calculation and the discussion are given in Section 3. Finally, the conclusion is presented in section 4.

2. Theoretical method

The CRM is one of the most useful simulation methods for the spectrum from the optically thin and isotropic plasma. It has been widely used to study

the spectrum of highly charged ions in X-ray, VUV and visible region[21–23]. In order to carry out the analysis of the fine structure of the spectrum, a detailed-level CRM should be used[22–25].

The spectral intensity $I_{i,j}(\lambda)$ of a transition from the upper level i to the lower level j with wavelength λ can be defined as:

$$I_{i,j}(\lambda) \propto n(i)A(i,j)\phi(\lambda). \quad (1)$$

where $A(i,j)$ is the transition rate for the transition from the energy level i to j , which can be obtained by experimental observations or by accurate theoretical calculations. The function $\phi(\lambda)$ is the normalized line profile, which was taken as a Gaussian profile to include the effect of Doppler, natural, collisional and instrumental broadenings in the present work. The notation $n(i)$ is the population of the ions in the excited upper level i , which was determined by the detailed atomic physics processes in the plasma, e.g., spontaneous radiative transitions, collisional excitation and deexcitation, collisional ionization, radiative recombination and three-body recombination etc.. These atomic processes can be calculated by using an appropriate theory.

For the plasma in the EBIT, which is in low electron density and the energy distribution of the free electron is almost mono-energy, the radiative recombination, three-body recombination, electron collisional ionization, and dielectronic recombination processes are expected to be negligible in this situation. Only the electron collisional excitations, deexcitations, and spontaneous radiative transitions processes will determine the population $n(i)$ of the excited upper level i . For a specifically excited level i , the temporal development of the population $n(i)$ can be obtained by solving the collisional-radiative rate equations:

$$\begin{aligned} \frac{d}{dt}n(i) &= \sum_{j<i} C(j,i)n_en(j) \\ &- [\sum_{j<i} F(i,j)n_e + A(i,j) + \sum_{j>i} C(i,j)n_e]n(i) \\ &+ \sum_{j>i} [F(j,i)n_e + A(j,i)]n(j). \end{aligned} \quad (2)$$

where n_e is the electron density of the plasma, $C(i,j)$ and $F(j,i)$ are collisional excitation and deexcitation rates coefficient from the level j to i , respectively.

These rate coefficient can be calculated by convoluting the cross section of the collisional (de) excitation processes with the free electron energy distribution function, which can be assumed as Maxwellian distribution, for the plasma in local thermodynamic equilibrium (LTE) with the electron temperature T_e . However, the electron energy distribution in the electron beam of the EBIT is more like mono-energy distribution function instead of Maxwellian distribution. Thus, the rate coefficient for the atomic processes in the EBIT may be calculated by taking the electron energy distribution as the δ function. These rate equations are solved under the Quasi-Steady-State (QSS) approximation, i.e., $dn(i)/dt = 0$. Finally, the intensity $I_{i,j}(\lambda)$ of the specific transition can be calculated when the population $n(i)$ of the upper level i of the transition is obtained.

Because the W^{54+} ion is a heavy highly charged ion, the relativistic effects will play an important role in the energy level structure and transition properties. The ground state of W^{54+} ion is $[Ne]3s^23p^63d^2$, which have two electrons in the open $3d$ subshells. Therefore, the relativistic and electron correlation effects should both be taken into account in the theoretical calculation. The present calculation is performed by using the relativistic configuration interaction (RCI) method with the implementation of FAC packages[26]. The atomic data including the energy levels, radiative transition rates, and cross sections of collisional (de) excitation are calculated. The collisional deexcitation process is the inverse of collisional excitation process. Therefore, the collisional deexcitation rate coefficient can be calculated by the principle of detailed balance from the corresponding electron collisional excitation process. In the present calculation, most of the important configuration interaction are included by single and double electron substitution from $n=3$ shells to $n=4$ subshells (nSD). For instance, the configuration interaction from configuration $3s^23p^63dnl(n=4)$, $3s^23p^53d^2nl(n=3, 4)$, $3s^13p^63d^2nl(n=3, 4)$, $3s^23p^6nln'l'(n, n'=4)$, $3s^23p^43d^2nln'l'(n, n'=3, 4)$, $3p^63d^2nln'l'(n, n'=3, 4)$, $3s^23p^53dln'l'(n, n'=3, 4)$, $3s^13p^63dln'l'(n, n'=3, 4)$ were taken into account in the present calculation. The E1 radiative transitions, electron collisional excitation processes between the levels of the

configuration $3p^63d^2$, $3p^53d^3$, $3p^63d4l$ are included to simulate the spectrum of W^{54+} ion.

3. Result and discussion

The level energies (in eV) of the ground state $3p^63d^2$ and the first excited state $3p^53d^3$ multiplets of W^{54+} ion were presented in Table 1. The levels are sorted by their excitation energies. There are 9 levels in the ground state $3p^63d^2$ and 110 levels in the first excited state $3p^53d^3$. The jj coupling labels are provided to designate the levels. The level energies calculated from different electron correlation models (nSD) are given to show the configuration interaction effects on the excitation energies. It can be inferred from the table that the level energies converge along with the increase of configurations interaction. The result of the present calculation agrees well with previous MCDF calculations[20]. The discrepancy was found to be about 0.12%. For the levels of ground configuration, the results from the NIST database[27] were compared with the present calculation. The discrepancy was about 0.19%. A good agreement between the present result and previous result was found indicating that the most of the important configuration interaction effects has been included in the present work.

Table 1. The level energies (in eV) of the ground state $3p^63d^2$ and the first excited state $3p^53d^3$ of W^{54+} ion. The column DF is the level energy calculated with Dirac-Hartree-Fock approximation. The fourth and fifth column labeled as cal(3SD) and cal(4SD) represent the level energy obtained by considering the configuration interaction from single and double substitution in $n=3$ and $n=4$ subshells. The column 'Theo.' and 'NIST' represent the previous available data obtained by MCDF calculation and the NIST database[27] for comparison.

Index	Levels	DF	cal(3SD)	cal(4SD)	Theo. ^a	NIST
<i>Groundstate</i> $3s^23p^63d^2$						
1	$[3p^63d_{3/2}^2]_2$	0	0	0	0	0
2	$[3p^63d_{3/2}^2]_0$	24.317	24.173	23.248	23.123	23.309
3	$[3p^63d_{3/2}3d_{5/2}]_3$	71.992	72.023	72.321	72.456	72.59
4	$[3p^63d_{3/2}3d_{5/2}]_2$	83.069	83.067	82.736	82.805	82.882

Continued...

Table 1 Continued...

Index	Levels	DF	cal(3SD)	cal(4SD)	Theo. ^a	NIST
5	$[3p^6 3d_{3/2} 3d_{5/2}]_4$	86.125	86.118	86.300	86.359	86.4
6	$[3p^6 3d_{3/2} 3d_{5/2}]_1$	88.161	88.138	87.597	87.613	87.962
7	$[3p^6 3d_{5/2}^2]_4$	152.557	152.596	152.933	153.158	153
8	$[3p^6 3d_{5/2}^2]_2$	161.371	161.384	160.966	161.160	161.1
9	$[3p^6 3d_{5/2}^2]_0$	186.754	186.482	185.041	185.140	185.5
<i>Excitedstate</i> $3s^2 3p^5 3d^3$						
10	$[(3p_{1/2}^2 3p_{3/2}^3)_{3/2} (3d_{5/2}^3)_{3/2}]_2$	271.864	267.172	273.656	273.769	
11	$[(3p_{1/2}^2 3p_{3/2}^3)_{3/2} (3d_{3/2}^3)_{3/2}]_1$	276.776	272.177	278.597	278.693	
12	$[(3p_{1/2}^2 3p_{3/2}^3)_{3/2} (3d_{3/2}^3)_{3/2}]_0$	281.019	276.325	282.713	282.774	
13	$[(3p_{1/2}^2 3p_{3/2}^3)_{3/2} (3d_{5/2}^3)_{3/2}]_3$	282.739	278.073	284.507	284.582	
14	$[(3p_{1/2}^2 3p_{3/2}^3)_{3/2} (3d_{3/2}^2)_{3/2} 3d_{5/2}]_3$	334.793	330.688	337.025	337.262	
15	$[(3p_{1/2}^2 3p_{3/2}^3)_{3/2} (3d_{3/2}^2)_{5/2} 3d_{5/2}]_4$	340.543	336.665	342.952	343.159	
16	$[(3p_{1/2}^2 3p_{3/2}^3)_{3/2} (3d_{3/2}^2)_{3/2} 3d_{5/2}]_2$	342.013	337.558	343.879	344.043	
17	$[(3p_{1/2}^2 3p_{3/2}^3)_{3/2} (3d_{3/2}^2)_{1/2} 3d_{5/2}]_2$	344.868	340.627	346.909	347.135	
18	$[(3p_{1/2}^2 3p_{3/2}^3)_{3/2} (3d_{3/2}^2)_{3/2} 3d_{5/2}]_1$	346.876	342.447	348.711	348.901	
19	$[(3p_{1/2}^2 3p_{3/2}^3)_{3/2} (3d_{3/2}^2)_{5/2} 3d_{5/2}]_5$	348.958	345.129	351.385	351.541	
20	$[(3p_{1/2}^2 3p_{3/2}^3)_{3/2} (3d_{3/2}^2)_{7/2} 3d_{5/2}]_3$	349.878	345.632	351.879	352.048	
21	$[(3p_{1/2}^2 3p_{3/2}^3)_{3/2} (3d_{3/2}^2)_{5/2} 3d_{5/2}]_0$	349.968	345.632	351.926	352.089	
22	$[(3p_{1/2}^2 3p_{3/2}^3)_{3/2} (3d_{3/2}^2)_{7/2} 3d_{5/2}]_6$	350.377	346.507	352.741	352.878	
23	$[(3p_{1/2}^2 3p_{3/2}^3)_{3/2} (3d_{3/2}^2)_{3/2} 3d_{5/2}]_4$	350.991	346.859	353.116	353.284	
24	$[(3p_{1/2}^2 3p_{3/2}^3)_{3/2} (3d_{3/2}^2)_{7/2} 3d_{5/2}]_4$	357.312	353.222	359.492	359.671	
25	$[(3p_{1/2}^2 3p_{3/2}^3)_{3/2} (3d_{3/2}^2)_{5/2} 3d_{5/2}]_2$	359.202	354.601	360.928	361.129	
26	$[(3p_{1/2}^2 3p_{3/2}^3)_{3/2} (3d_{3/2}^2)_{5/2} 3d_{5/2}]_3$	359.647	355.507	361.754	361.952	
27	$[(3p_{1/2}^2 3p_{3/2}^3)_{3/2} (3d_{3/2}^2)_{5/2} 3d_{5/2}]_1$	359.997	355.537	361.840	362.029	
28	$[(3p_{1/2}^2 3p_{3/2}^3)_{3/2} (3d_{3/2}^2)_{7/2} 3d_{5/2}]_5$	365.560	361.917	368.102	368.256	
29	$[(3p_{1/2}^2 3p_{3/2}^3)_{3/2} (3d_{3/2}^2)_{3/2} 3d_{5/2}]_4$	377.203	372.566	378.857	378.929	
30	$[(3p_{1/2}^2 3p_{3/2}^3)_{3/2} (3d_{3/2}^2)_{3/2} 3d_{5/2}]_2$	381.494	376.402	382.637	382.657	
31	$[(3p_{1/2}^2 3p_{3/2}^3)_{3/2} (3d_{3/2}^2)_{7/2} 3d_{5/2}]_1$	390.190	383.853	390.051	390.056	
32	$[(3p_{1/2}^2 3p_{3/2}^3)_{3/2} (3d_{3/2}^2)_{3/2} 3d_{5/2}]_3$	390.357	384.849	390.889	390.731	
33	$[(3p_{1/2}^2 3p_{3/2}^3)_{3/2} (3d_{3/2}^2)_{5/2} 3d_{5/2}]_2$	393.665	387.333	393.325	393.157	
34	$[(3p_{1/2}^2 3p_{3/2}^3)_{3/2} (3d_{3/2}^2)_{3/2} 3d_{5/2}]_3$	395.220	388.874	394.857	394.733	
35	$[[(3p_{1/2}^2 3p_{3/2}^3)_{3/2} 3d_{3/2}]_0 (3d_{5/2}^2)_4]_4$	410.421	406.464	412.697	413.038	
36	$[[(3p_{1/2}^2 3p_{3/2}^3)_{3/2} 3d_{3/2}]_1 (3d_{5/2}^2)_4]_5$	414.800	411.268	417.424	417.736	
37	$[[(3p_{1/2}^2 3p_{3/2}^3)_{3/2} 3d_{3/2}]_0 (3d_{5/2}^2)_2]_2$	416.667	412.128	418.373	418.689	
38	$[[(3p_{1/2}^2 3p_{3/2}^3)_{3/2} (3d_{3/2}^2)_0]_{3/2} 3d_{5/2}]_1$	418.451	414.824	420.451	419.866	
39	$[[(3p_{1/2}^2 3p_{3/2}^3)_{3/2} 3d_{3/2}]_3 (3d_{5/2}^2)_4]_6$	420.957	415.297	421.437	421.736	
40	$[[(3p_{1/2}^2 3p_{3/2}^3)_{3/2} 3d_{3/2}]_1 (3d_{5/2}^2)_4]_3$	425.424	421.069	427.235	427.500	
41	$[[(3p_{1/2}^2 3p_{3/2}^3)_{3/2} 3d_{3/2}]_3 (3d_{5/2}^2)_2]_2$	425.944	422.356	428.549	428.802	
42	$[[(3p_{1/2}^2 3p_{3/2}^3)_{3/2} 3d_{3/2}]_3 (3d_{5/2}^2)_4]_5$	425.991	422.467	428.574	428.881	
43	$[[(3p_{1/2}^2 3p_{3/2}^3)_{3/2} 3d_{3/2}]_1 (3d_{5/2}^2)_2]_1$	426.923	422.600	428.819	429.044	
44	$[[(3p_{1/2}^2 3p_{3/2}^3)_{3/2} 3d_{3/2}]_3 (3d_{5/2}^2)_4]_7$	427.623	423.133	429.239	429.467	
45	$[[(3p_{1/2}^2 3p_{3/2}^3)_{3/2} 3d_{3/2}]_1 (3d_{5/2}^2)_4]_4$	427.672	423.334	429.534	429.789	

Continued...

Table 1 Continued...

Index	Levels	DF	cal(3SD)	cal(4SD)	Theo. ^a	NIST
46	$[(3p_{1/2}^2 3p_{3/2}^3)_{3/2} 3d_{3/2}]_1 (3d_{5/2}^2)_2]_3$	432.445	427.718	433.929	434.203	
47	$[(3p_{1/2}^2 3p_{3/2}^3)_{3/2} 3d_{3/2}]_2 (3d_{5/2}^2)_4]_4$	437.602	433.178	439.202	439.326	
48	$[(3p_{1/2}^2 3p_{3/2}^3)_{3/2} 3d_{3/2}]_2 (3d_{5/2}^2)_4]_3$	438.543	434.006	440.144	440.334	
49	$[(3p_{1/2}^2 3p_{3/2}^3)_{3/2} 3d_{3/2}]_3 (3d_{5/2}^2)_2]_1$	438.641	434.784	441.037	441.338	
50	$[(3p_{1/2}^2 3p_{3/2}^3)_{3/2} 3d_{3/2}]_2 (3d_{5/2}^2)_4]_6$	439.931	435.500	441.552	441.773	
51	$[(3p_{1/2}^2 3p_{3/2}^3)_{3/2} 3d_{3/2}]_3 (3d_{5/2}^2)_2]_4$	440.325	435.762	441.869	442.007	
52	$[(3p_{1/2}^2 3p_{3/2}^3)_{3/2} 3d_{3/2}]_3 (3d_{5/2}^2)_2]_5$	440.336	436.009	442.079	442.165	
53	$[(3p_{1/2}^2 3p_{3/2}^3)_{3/2} 3d_{3/2}]_0 (3d_{5/2}^2)_0]_0$	444.847	439.450	445.855	446.163	
54	$[(3p_{1/2}^2 3p_{3/2}^3)_{3/2} 3d_{3/2}]_2 (3d_{5/2}^2)_2]_2$	447.059	442.116	448.282	448.481	
55	$[(3p_{1/2}^2 3p_{3/2}^3)_{3/2} 3d_{3/2}]_3 (3d_{5/2}^2)_4]_3$	452.440	447.295	453.385	453.580	
56	$[(3p_{1/2}^2 3p_{3/2}^3)_{3/2} 3d_{3/2}]_3 (3d_{5/2}^2)_4]_4$	456.750	451.980	458.032	458.198	
57	$[(3p_{1/2}^2 3p_{3/2}^3)_{3/2} 3d_{3/2}]_2 (3d_{5/2}^2)_4]_2$	460.988	455.504	461.538	461.647	
58	$[(3p_{1/2}^2 3p_{3/2}^3)_{3/2} 3d_{3/2}]_2 (3d_{5/2}^2)_4]_5$	464.235	459.539	465.368	465.389	
59	$[(3p_{1/2}^2 3p_{3/2}^3)_{3/2} 3d_{3/2}]_1 (3d_{5/2}^2)_0]_1$	465.621	460.007	466.285	466.474	
60	$[(3p_{1/2}^2 3p_{3/2}^3)_{3/2} 3d_{3/2}]_3 (3d_{5/2}^2)_0]_3$	470.088	464.555	470.752	470.828	
61	$[(3p_{1/2}^2 3p_{3/2}^3)_{3/2} 3d_{3/2}]_3 (3d_{5/2}^2)_4]_2$	471.224	466.182	471.920	471.719	
62	$[(3p_{1/2}^2 3p_{3/2}^3)_{3/2} 3d_{3/2}]_3 (3d_{5/2}^2)_4]_1$	474.370	467.146	473.333	473.503	
63	$[(3p_{1/2}^2 3p_{3/2}^3)_{3/2} 3d_{3/2}]_2 (3d_{5/2}^2)_0]_2$	474.387	468.779	474.956	475.067	
64	$[(3p_{1/2}^2 3p_{3/2}^3)_{3/2} 3d_{3/2}]_2 (3d_{5/2}^2)_2]_3$	476.453	469.685	475.569	475.534	
65	$[(3p_{1/2}^2 3p_{3/2}^3)_{3/2} 3d_{3/2}]_3 (3d_{5/2}^2)_2]_4$	477.385	470.400	476.323	476.313	
66	$[(3p_{1/2}^2 3p_{3/2}^3)_{3/2} 3d_{3/2}]_2 (3d_{5/2}^2)_0]_2$	481.909	475.078	480.941	480.731	
67	$[(3p_{1/2}^2 3p_{3/2}^3)_{3/2} 3d_{3/2}]_1 (3d_{5/2}^2)_2]_1$	486.173	479.787	485.476	485.082	
68	$[(3p_{1/2}^2 3p_{3/2}^3)_{3/2} 3d_{3/2}]_2 (3d_{5/2}^2)_2]_0$	486.665	481.009	486.558	486.092	
69	$[(3p_{1/2}^2 3p_{3/2}^3)_{3/2} 3d_{3/2}]_3 (3d_{5/2}^2)_2]_3$	487.142	482.322	487.985	487.630	
70	$[(3p_{1/2}^2 3p_{3/2}^3)_{3/2} (3d_{5/2}^3)_9]_2]_6$	493.589	490.274	496.363	496.802	
71	$[(3p_{1/2}^2 3p_{3/2}^3)_{3/2} (3d_{5/2}^3)_3]_2]_0$	504.879	500.470	506.656	507.002	
72	$[(3p_{1/2}^2 3p_{3/2}^3)_{3/2} (3d_{5/2}^3)_9]_2]_5$	505.289	500.800	506.733	507.038	
73	$[(3p_{1/2}^2 3p_{3/2}^3)_{3/2} (3d_{5/2}^3)_3]_2]_3$	506.786	502.182	508.242	508.543	
74	$[(3p_{1/2}^2 3p_{3/2}^3)_{3/2} (3d_{5/2}^3)_3]_2]_2$	523.308	517.979	524.093	524.365	
75	$[(3p_{1/2}^2 3p_{3/2}^3)_{3/2} (3d_{5/2}^3)_5]_2]_4$	524.286	519.340	525.606	525.942	
76	$[(3p_{1/2}^2 3p_{3/2}^3)_{3/2} (3d_{5/2}^3)_5]_2]_2$	535.660	530.254	536.143	536.137	
77	$[(3p_{1/2}^2 3p_{3/2}^3)_{3/2} (3d_{5/2}^3)_9]_2]_4$	540.624	534.476	540.343	540.525	
78	$[(3p_{1/2}^2 3p_{3/2}^3)_{3/2} (3d_{5/2}^3)_5]_2]_3$	544.344	538.414	544.495	544.801	
79	$[(3p_{1/2}^2 3p_{3/2}^3)_{3/2} (3d_{5/2}^3)_5]_2]_3$	553.354	548.107	553.875	553.794	
80	$[(3p_{1/2}^2 3p_{3/2}^3)_{3/2} (3d_{5/2}^3)_3]_2]_1$	556.678	550.699	556.634	556.773	
81	$[(3p_{1/2}^2 3p_{3/2}^3)_{3/2} (3d_{5/2}^3)_5]_2]_1$	567.604	558.998	565.219	565.442	
82	$[(3p_{1/2} 3p_{3/2}^4)_{1/2} (3d_{3/2}^3)_3]_2]_2$	632.534	626.627	632.604	632.492	
83	$[(3p_{1/2} 3p_{3/2}^4)_{1/2} (3d_{3/2}^3)_3]_2]_1$	669.418	660.920	666.964	666.827	
84	$[(3p_{1/2} 3p_{3/2}^4)_{1/2} (3d_{3/2}^2)_2]_{5/2} 3d_{5/2}]_3$	685.896	680.855	686.909	687.221	
85	$[(3p_{1/2} 3p_{3/2}^4)_{1/2} (3d_{3/2}^2)_2]_{5/2} 3d_{5/2}]_2$	686.471	681.280	687.301	687.555	
86	$[(3p_{1/2} 3p_{3/2}^4)_{1/2} (3d_{3/2}^2)_2]_{5/2} 3d_{5/2}]_1$	691.022	685.843	691.842	692.014	
87	$[(3p_{1/2} 3p_{3/2}^4)_{1/2} (3d_{3/2}^2)_2]_{5/2} 3d_{5/2}]_4$	692.811	687.884	693.899	694.156	

Continued...

Table 1 Continued...

Index	Levels	DF	cal(3SD)	cal(4SD)	Theo. ^a	NIST
88	$[(3p_{1/2}3p_{3/2}^4)_{1/2}(3d_{3/2}^2)_{5/2}3d_{5/2}]_0$	693.116	688.045	694.040	694.211	
89	$[(3p_{1/2}3p_{3/2}^4)_{1/2}(3d_{3/2}^2)_{5/2}3d_{5/2}]_5$	694.625	690.205	696.166	696.384	
90	$[(3p_{1/2}3p_{3/2}^4)_{1/2}(3d_{3/2}^2)_{0}1/23d_{5/2}]_2$	726.627	720.330	726.189	726.150	
91	$[(3p_{1/2}3p_{3/2}^4)_{1/2}(3d_{3/2}^2)_{3/2}3d_{5/2}]_3$	731.048	724.068	729.856	729.825	
92	$[(3p_{1/2}3p_{3/2}^4)_{1/2}(3d_{3/2}^2)_{3/2}3d_{5/2}]_4$	738.006	730.188	735.993	735.966	
93	$[(3p_{1/2}3p_{3/2}^4)_{1/2}(3d_{3/2}^2)_{3/2}3d_{5/2}]_2$	739.656	732.355	738.170	738.129	
94	$[(3p_{1/2}3p_{3/2}^4)_{1/2}(3d_{3/2}^2)_{3/2}3d_{5/2}]_1$	743.215	734.282	740.378	740.497	
95	$[(3p_{1/2}3p_{3/2}^4)_{1/2}(3d_{3/2}^2)_{0}1/23d_{5/2}]_3$	744.170	738.029	743.776	743.576	
96	$[(3p_{1/2}3p_{3/2}^4)_{1/2}(3d_{3/2}^2)_{3/2}2(3d_{5/2}^2)_{4}]_4$	752.738	748.314	754.373	754.976	
97	$[(3p_{1/2}3p_{3/2}^4)_{1/2}(3d_{3/2}^2)_{3/2}2(3d_{5/2}^2)_{4}]_3$	756.827	751.744	757.770	758.279	
98	$[(3p_{1/2}3p_{3/2}^4)_{1/2}(3d_{3/2}^2)_{3/2}2(3d_{5/2}^2)_{4}]_5$	759.325	755.182	761.205	761.763	
99	$[(3p_{1/2}3p_{3/2}^4)_{1/2}(3d_{3/2}^2)_{3/2}2(3d_{5/2}^2)_{2}]_0$	763.576	758.015	764.190	764.767	
100	$[(3p_{1/2}3p_{3/2}^4)_{1/2}(3d_{3/2}^2)_{3/2}2(3d_{5/2}^2)_{2}]_1$	763.984	758.436	764.604	765.173	
101	$[(3p_{1/2}3p_{3/2}^4)_{1/2}(3d_{3/2}^2)_{3/2}2(3d_{5/2}^2)_{4}]_2$	764.909	759.220	765.349	765.853	
102	$[(3p_{1/2}3p_{3/2}^4)_{1/2}(3d_{3/2}^2)_{3/2}2(3d_{5/2}^2)_{2}]_2$	766.354	760.652	766.765	767.260	
103	$[(3p_{1/2}3p_{3/2}^4)_{1/2}(3d_{3/2}^2)_{3/2}2(3d_{5/2}^2)_{4}]_6$	769.565	765.786	771.778	772.272	
104	$[(3p_{1/2}3p_{3/2}^4)_{1/2}(3d_{3/2}^2)_{3/2}2(3d_{5/2}^2)_{2}]_4$	773.439	768.403	774.429	774.884	
105	$[(3p_{1/2}3p_{3/2}^4)_{1/2}(3d_{3/2}^2)_{3/2}2(3d_{5/2}^2)_{2}]_3$	776.986	771.433	777.559	778.043	
106	$[(3p_{1/2}3p_{3/2}^4)_{1/2}(3d_{3/2}^2)_{3/2}2(3d_{5/2}^2)_{0}]_2$	796.183	789.842	796.082	796.470	
107	$[(3p_{1/2}3p_{3/2}^4)_{1/2}(3d_{3/2}^2)_{3/2}1(3d_{5/2}^2)_{4}]_5$	797.381	791.151	796.687	796.760	
108	$[(3p_{1/2}3p_{3/2}^4)_{1/2}(3d_{3/2}^2)_{3/2}1(3d_{5/2}^2)_{4}]_4$	798.948	792.159	797.999	798.247	
109	$[(3p_{1/2}3p_{3/2}^4)_{1/2}(3d_{3/2}^2)_{3/2}1(3d_{5/2}^2)_{2}]_3$	803.296	796.136	802.009	802.234	
110	$[(3p_{1/2}3p_{3/2}^4)_{1/2}(3d_{3/2}^2)_{3/2}1(3d_{5/2}^2)_{2}]_1$	806.282	798.409	804.420	804.706	
111	$[(3p_{1/2}3p_{3/2}^4)_{1/2}(3d_{3/2}^2)_{3/2}1(3d_{5/2}^2)_{4}]_3$	811.530	805.282	810.977	810.831	
112	$[(3p_{1/2}3p_{3/2}^4)_{1/2}(3d_{3/2}^2)_{3/2}1(3d_{5/2}^2)_{2}]_2$	812.190	805.501	811.002	811.046	
113	$[(3p_{1/2}3p_{3/2}^4)_{1/2}(3d_{3/2}^2)_{3/2}1(3d_{5/2}^2)_{0}]_1$	831.396	823.862	829.747	829.814	
114	$[(3p_{1/2}3p_{3/2}^4)_{1/2}(3d_{5/2}^3)_{9/2}]_4$	831.475	826.499	832.469	833.226	
115	$[(3p_{1/2}3p_{3/2}^4)_{1/2}(3d_{5/2}^3)_{9/2}]_5$	840.088	835.570	841.539	842.263	
116	$[(3p_{1/2}3p_{3/2}^4)_{1/2}(3d_{5/2}^3)_{3/2}]_1$	851.857	845.181	851.236	851.798	
117	$[(3p_{1/2}3p_{3/2}^4)_{1/2}(3d_{5/2}^3)_{3/2}]_2$	852.971	847.109	853.197	853.855	
118	$[(3p_{1/2}3p_{3/2}^4)_{1/2}(3d_{5/2}^3)_{5/2}]_2$	859.833	853.175	859.378	860.010	
119	$[(3p_{1/2}3p_{3/2}^4)_{1/2}(3d_{5/2}^3)_{5/2}]_3$	864.667	858.388	864.592	865.208	

^aFrom Ding et al by MCDF method[20].

According to the present calculation, the wavelength of E1 transition from the first excited state $3s^23p^53d^3$ to the ground configuration state $3s^23p^63d^2$ covered the range of 18.5-32.5 Å. The strong transition with large transition rates was concentrated in two wavelength range 29.5-32.5 Å and 18.5-19.6 Å.

The transition wavelength λ (in Å), transition rate A (in s⁻¹), population

$n(i)$ and intensity $I_{ij}(\lambda)$ of E1 transition from $3s^23p^53d^3$ to $3s^23p^63d^2$ of W^{54+} ion are presented for a wavelength range from 29.5-32.5 Å in Table 2. The experimental value observed by EBIT and the theoretical values from FAC[26] and MCDF[11, 12] are also included for comparison. The present calculation agrees quite well with the experimental data and other theoretical values. The wavelength discrepancy between T. Lennartsson *et al.* [13] by experiment, Dipti *et al.* [12] and Ding *et al.* [11] by MCDF method, T. Lennartsson *et al.* [13] by FAC calculations and the present calculation are about 0.25%, 0.14%, 0.11% and 0.07%, respectively. All the observed transition lines from the EBIT experiment were identified in the present calculation. It was found that the observed transition lines in the EBIT experiment have large transition rates. However, a few transitions in this range with large transition rates have not been observed in the previous EBIT experiment, such as transitions with the key 7, 8 and 9. The reason is the population (Pop) of the excited upper levels of these unobserved transitions is extremely small. The results show that the intensity (Int) of the unobserved transitions are generally smaller by four orders of magnitude than the intensity which could be observed. The intensity might be changed with the plasma conditions. It can be expected that these unobserved strong transitions might be observed by the appropriate plasma condition.

The synthetic spectrum of W^{54+} ion in the wavelength 29.5-32.5 Å is shown in Fig. 1. Each individual transition was assumed to have the Gaussian profile with full width at half maximum (FWHM) 0.09 Å. The upper part Fig. 1(a) is the spectrum obtained by convoluting the transition rate, while the middle part Fig. 1(b) is the spectrum by considering the population of the upper level in the EBIT case with the electron density $n_e = 10^{12} \text{ cm}^{-3}$ and the energy of electron beam $E_e = 18.2 \text{ keV}$. All 7 peaks observed by the experimental observation[13] can be reproduced by the synthetic spectrum. The lower part Fig. 1(c) is the spectrum by considering the excited upper levels in the LTE plasma with the electron density $n_e = 10^{15} \text{ cm}^{-3}$ and the electron temperature $T_e = 18.2 \text{ keV}$, and the electron energy distribution is Maxwellian. The results indicate that all the strong transition lines are observable under this plasma condition.

Table 2. The calculated transition wavelength λ (Å), transition rate A (in s^{-1}), population (Pop), intensity (Int) and available experimental and other theoretical values for the strong E1 transition of W^{54+} ion. The column 'Key' correspond to the label in figure 1. Notion $a(b)$ for transition probabilities A means $a \times 10^b$.

Lower	Upper	$\lambda(\text{Å})$	$\lambda_{others}(\text{Å})$	$A(/s^{-1})$	$A^c(/s^{-1})$	Pop	Int	Key
1	30	32.403	32.264 ^a 32.502 ^b 32.401 ^c 32.416 ^d	8.30(10)	8.50(10)	6.92(-14)	5.74(-3)	1
1	31	31.787	31.811 ^a 31.783 ^b 31.787 ^c 31.786 ^d	7.49(11)	7.44(11)	3.63(-14)	2.72(-2)	2
1	32	31.719	31.776 ^a 31.765 ^b 31.732 ^c 31.711 ^d	5.43(11)	5.91(11)	9.05(-14)	4.92(-2)	3
1	33	31.522	31.563 ^a 31.503 ^b 31.536 ^c 31.505 ^d	9.60(11)	9.43(11)	6.35(-14)	6.09(-2)	4
1	34	31.400	31.430 ^a 31.378 ^b 31.410 ^c 31.386 ^d	5.89(11)	5.18(11)	8.80(-14)	5.18(-2)	5
2	38	31.215	31.245 ^a 31.236 ^b 31.251 ^c 31.155 ^d	9.39(11)	9.33(11)	7.75(-15)	7.28(-3)	6
6	68	31.077	31.115 ^c	1.18(12)	1.16(12)	8.68(-20)	1.03(-7)	7
7	79	30.924	30.948 ^c	1.19(12)	1.17(12)	1.88(-20)	2.23(-8)	8
5	69	30.866	30.898 ^c	1.19(12)	1.16(12)	3.26(-16)	3.86(-4)	9
1	38	29.489	29.560 ^a 29.456 ^b 29.530 ^c 29.452 ^d	3.08(11)	2.96(11)	7.75(-15)	2.39(-3)	10

^a From T. Lennartsson by EBIT experiment[13].

^b From Dipti et al by MCDF method[12].

^c From Ding et al by MCDF method[11].

^d From T. Lennartsson by collisional-radiative model[13]

The large difference between Fig. 1 (b) and (c) is caused by the dependence of population mechanism on the free electron energy distribution function in a different plasma environment. The intensity for a specific transition line is proportion to the population of the excited upper level i which will be populated by the collisional excitation processes from other lower energy levels and collisional deexcitation processes from other higher energy levels (referenced as population flux), and will be depopulated by the collisional excitation processes to other higher energy levels and collisional deexcitation processes to other lower energy levels (referenced as depopulation flux). Collisional excitation and deexcitation rates coefficient are obtained by convoluting the cross section of the corresponding collisional (de)excitation processes with the free electron energy distribution function (EEDF) in the plasma. In the present work, the EEDF in the EBIT plasma and LTE plasma are taken as the δ function and the Maxwellian distribution function, respectively. In the EBIT plasma, for example, the strong transition line have been observed in the previous EBIT experiment with the key 4, the ratio of the population flux and depopulation flux of the excited upper level is 1.12, while the weak transition line which have not been observed in the previous EBIT experiment with the key 9, the ratio of the population flux and depopulation flux is 0.15. This means the excited upper level of the weak peak have a small population compare with the strong peak. In the LTE plasma, for all excited upper levels, the ratio of the population flux and depopulation flux about are 0.07, which means the population for the excited upper levels almost same. Thus the intensity only proportional to the transition rates. As a result, the transition 7, 8 and 9 are large enough to be observed.

The wavelength λ (in \AA), transition rate A (in s^{-1}), population $n(i)$ and intensity $I_{ij}(\lambda)$ of E1 transition $3s^23p^53d^3$ to $3s^23p^63d^2$ in the wavelength range 18.5-19.6 \AA are presented in Table 3. The theoretical values from MCDF calculation[11] are also included for comparison. The present calculation values generally made a good agreement with the previous data. The wavelength discrepancy was found to be about 0.04%. According to the present calculation, some strong transitions may be observed in the wavelength range of 18.5-19.6

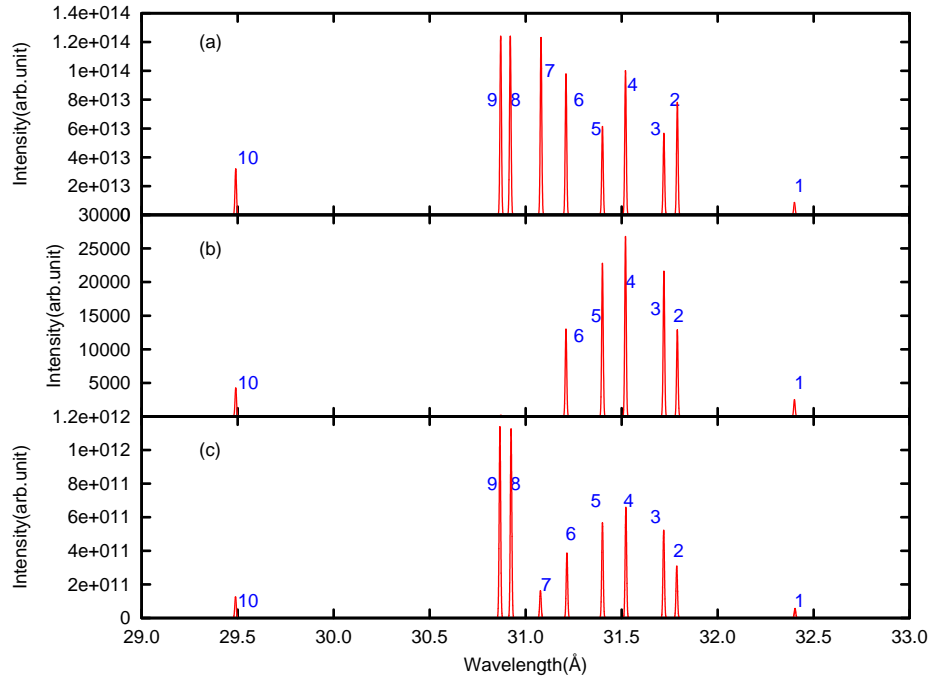


Fig. 1. The synthetic spectrum of W^{54+} ion in wavelength 29.5-32.5 Å. (a).convoluting the transition rate with the Gaussian profile; (b).the spectrum for the EBIT case with $n_e = 10^{12} \text{ cm}^{-3}$ and $E_e = 18.2 \text{ keV}$; (c).the spectrum for the LTE plasma with $n_e = 10^{15} \text{ cm}^{-3}$ and $T_e = 18.2 \text{ keV}$.

Å. The synthetic spectrum of W^{54+} ion in this wavelength range was shown in Fig. 2. All the peaks were obtained with $FWHM = 0.05$ Å for each individually transition to make the spectrum clear. The upper part Fig. 2(a) is the spectrum obtained by convoluting the transition rate with the Gaussian profile. The middle part Fig. 2(b) is the spectrum by considering the population of the upper levels in the EBIT case with $n_e = 10^{12}$ cm^{-3} and $E_e = 18.2$ keV. According to the synthetic spectrum there are only 3 peaks that would be observed in the EBIT experiment with this condition, namely, the transition lines with key 1, 5, and 20 in Fig. 2(b), These 3 peaks are regarded as the E1 transition $[(3p_{1/2}3p_{3/2}^4)_{1/2}(3d_{3/2}^3)_{3/2}]_2 \rightarrow [3p^63d_{3/2}^2]_2$, $[(3p_{1/2}3p_{3/2}^4)_{1/2}(3d_{3/2}^3)_{3/2}]_1 \rightarrow [3p^63d_{3/2}^2]_0$, $[(3p_{1/2}3p_{3/2}^4)_{1/2}(3d_{3/2}^3)_{3/2}]_1 \rightarrow [3p^63d_{3/2}^2]_2$ with transition wavelength 19.599 Å, 19.260 Å and 18.590 Å, respectively. The lower part Fig. 2(c) is the spectrum by considering the population of the upper levels in the LTE plasma with $n_e = 10^{15}$ cm^{-3} and $T_e = 18.2$ keV, and the electron energy distribution is Maxwellian. The results indicate that all transition lines are observable in this condition. The difference between Fig. 2 (b) and (c) are caused by the same reason as in Fig. 1.

4. Conclusion

The energy level, E1 transition rate, and electron collisional excitation of the ground state $3s^23p^63d^2$ and the first excited state $3s^23p^53d^3$ of W^{54+} ion were calculated by relativistic configuration interaction method. A collisional-radiative model (CRM) was constructed to simulate the E1 transition spectrum for the EBIT and the LTE plasma. All the necessary atomic data for constructing the CRM was calculated by FAC packages. The most important configuration interaction effects were taken into account. The energy levels and transition rates made a reasonable agreement with the EBIT experimental observation and the previous theoretical values. The synthetic spectrum from the CRM explained the EBIT observation in the 29.5-32.5 Å. Furthermore, some possible transitions were proposed to be observed in 18.5-19.6 Å of the future the

Table 3. The calculated transition wavelength λ (\AA), transition rate A (in s^{-1}), population (Pop), intensity (Int) and the theoretical values from MCDF calculation for the strong E1 transition of W^{54+} ion. The column 'Key' correspond to the label in figure 2. Notion $a(b)$ for transition probabilities A means $a \times 10^b$.

Lower	Upper	$\lambda(\text{\AA})$	$\lambda^a(\text{\AA})$	$A(/s^{-1})$	$A^a(/s^{-1})$	Pop	Int	Key
1	82	19.599	19.603	2.95(12)	2.88(12)	1.31(-14)	3.85(-2)	1
8	109	19.341	19.340	1.66(12)	1.61(12)	1.32(-19)	2.19(-7)	2
8	110	19.269	19.266	4.09(12)	4.03(12)	2.58(-18)	1.06(-5)	3
7	107	19.261	19.264	2.85(12)	2.79(12)	9.40(-20)	2.68(-7)	4
2	83	19.260	19.261	1.78(12)	1.76(12)	4.86(-15)	8.64(-3)	5
9	113	19.231	19.232	2.81(12)	2.79(12)	1.84(-17)	5.15(-5)	6
7	108	19.221	19.220	3.36(12)	3.30(12)	5.78(-19)	1.94(-6)	7
4	91	19.160	19.162	1.96(12)	1.93(12)	3.71(-17)	7.26(-5)	8
7	109	19.102	19.102	2.14(12)	2.13(12)	1.32(-19)	2.82(-7)	9
5	92	19.084	19.086	4.59(12)	4.52(12)	2.44(-17)	1.12(-4)	10
8	111	19.074	19.084	1.46(12)	1.45(12)	6.80(-19)	9.90(-7)	11
8	112	19.074	19.078	3.10(12)	3.00(12)	1.06(-17)	3.29(-5)	12
6	93	19.058	19.060	2.63(12)	2.60(12)	2.11(-17)	5.55(-5)	13
6	94	18.993	18.991	1.66(12)	1.64(12)	1.66(-17)	2.74(-5)	14
3	90	18.962	18.967	4.08(12)	3.97(12)	4.48(-17)	1.83(-4)	15
5	95	18.858	18.865	4.35(12)	4.24(12)	1.86(-17)	8.11(-5)	16
3	91	18.856	18.861	1.99(12)	1.96(12)	3.71(-17)	7.40(-5)	17
4	94	18.853	18.852	4.55(12)	4.48(12)	1.66(-17)	7.55(-5)	18
7	111	18.842	18.852	2.25(12)	2.15(12)	6.80(-19)	1.53(-6)	19
1	83	18.590	18.594	5.18(12)	5.09(12)	4.86(-15)	2.52(-2)	20

^aFrom Ding et al by MCDF method[11].

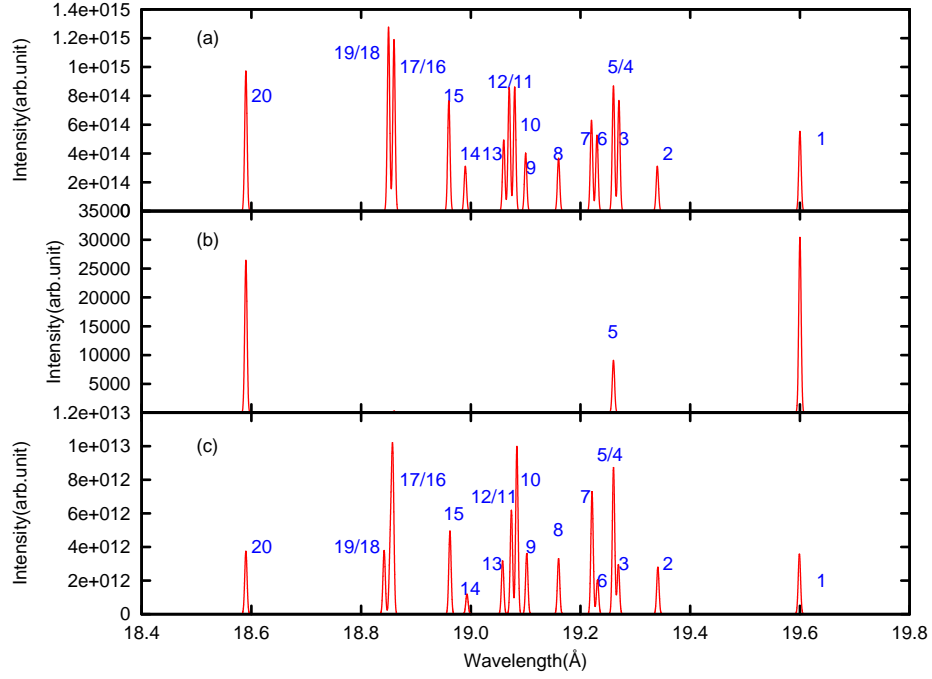


Fig. 2. The synthetic spectrum of W^{54+} ion in wavelength 18.5-19.6 Å. (a).convoluting the transition rate with the Gaussian profile; (b).the spectrum for the EBIT case with $n_e = 10^{12} \text{ cm}^{-3}$ and $E_e = 18.2 \text{ keV}$; (c).the spectrum for the LTE plasma with $n_e = 10^{15} \text{ cm}^{-3}$ and $T_e = 18.2 \text{ keV}$.

EBIT observations. Finally, the difference of the spectrum in different plasma condition was observed and explained.

Acknowledgment

This work was supported by National Key Research and Development Program of China, Grant No:NYK0123, National Nature Science Foundation of China, Grant No: 11264035, Specialized Research Fund for the Doctoral Program of Higher Education (SRFDP), Grant No: 20126203120004, International Scientific and Technological Cooperative Project of Gansu Province of China (Grant No. 1104WCGA186), JSPS-NRF-NSFC A3 Foresight Program in the field of Plasma Physics (NSFC: No. 11261140328, NRF: 2012K2A2A6000443).

References

References

- [1] R. Neu, R. Dux, A. Kallenbach, T. Pütterich, M. Balden, J. Fuchs, A. Herrmann, C. Maggi, M. O'Mullane, R. Pugno, I. Radivojevic, V. Rohde, A. Sips, W. Suttrop, A. Whiteford, the ASDEX Upgrade team, Tungsten: an option for divertor and main chamber plasma facing components in future fusion devices, Nucl. Fusion 45 (3) (2005) 209. doi:10.1088/0029-5515/45/3/007.
- [2] G. Matthews, P. Coad, H. Greuner, M. Hill, T. Hirai, J. Likonen, H. Maier, M. Mayer, R. Neu, V. Philipps, R. Pitts, V. Riccardo, Development of divertor tungsten coatings for the JET ITER-like wall, J. Nucl. Mater. 390 - 391 (2009) 934 - 937. doi:10.1016/j.jnucmat.2009.01.239.
- [3] R. Radtke, C. Biedermann, J. L. Schwob, P. Mandelbaum, R. Doron, Line and band emission from tungsten ions with charge 21+ to 45+ in the 45 - 70 Å range, Phys. Rev. A 64 (2001) 012720. doi:10.1103/PhysRevA.64.012720.
- [4] C. H. Skinner, Atomic physics in the quest for fusion energy and ITER, Phys. Scr. 2009 (T134) (2009) 014022. doi:10.1088/0031-8949/2009/T134/014022.
- [5] Z. Fei, W. Li, J. Grumer, Z. Shi, R. Zhao, T. Brage, S. Huldt, K. Yao, R. Hutton, Y. Zou, Forbidden-line spectroscopy of the ground-state configuration of Cd-like W, Phys. Rev. A 90 (2014) 052517. doi:10.1103/PhysRevA.90.052517.

- [6] A. E. Kramida, J. Reader, Ionization energies of tungsten ions: W^{2+} through W^{71+} , *At. Data Nucl. Data Tables* 92 (4) (2006) 457 – 479. doi:10.1016/j.adt.2006.03.002.
- [7] A. Kramida, T. Shirai, Energy levels and spectral lines of tungsten, W III through W LXXIV, *At. Data Nucl. Data Tables* 95 (3) (2009) 305–474. doi:10.1016/j.adt.2008.12.002.
- [8] A. Kramida, Recent progress in spectroscopy of tungsten, *Can. J. Phys.* 89 (2011) 551 – 570. doi:10.1139/p11-045.
- [9] M. B. Chowdhuri, S. Morita, M. Goto, H. Nishimura, K. Nagai, S. Fujioka, Line analysis of EUV spectra from molybdenum and tungsten injected with impurity pellets in LHD, *Plasma Fusion Res.* 2 (2007) S1060–S1060. doi:10.1585/pfr.2.S1060.
- [10] X.-B. Ding, F. Koike, I. Murakami, D. Kato, H. A. Sakaue, C.-Z. Dong, N. Nakamura, M1 transition energies and probabilities between the multiplets of the ground state of Ag-like ions with $Z = 47-92$, *J. Phys. B: At., Mol. Opt. Phys.* 45 (3) (2012) 035003. doi:10.1088/0953-4075/45/3/035003.
- [11] X. Ding, S. Rui, J. Liu, K. Fumihito, I. Murakami, D. Kato, H. A. Sakaue, N. Nakamura, C. Dong, E1, M1, E2 transition energies and probabilities of W^{54+} ions, *J. Phys. B: At., Mol. Opt. Phys.* 50 (4) (2017) 045004. doi:10.1088/1361-6455/aa53ec.
- [12] Dipti, T. Das, L. Sharma, R. Srivastava, Electron impact excitation and polarization studies of Fe-like W^{48+} to Al-like W^{61+} ions, *Can. J. Phys.* 93 (8) (2015) 888–897. doi:10.1088/0953-4075/47/17/175002.
- [13] T. Lennartsson, J. Clementson, P. Beiersdorfer, Experimental wavelengths for intrashell transitions in tungsten ions with partially filled $3p$ and $3d$ subshells, *Phys. Rev. A* 87 (2013) 062505. doi:10.1088/0953-4075/45/3/035003.
- [14] Y. Ralchenko, I. N. Draganic, J. N. Tan, J. D. Gillaspay, J. M. Pomeroy, J. Reader, U. Feldman, G. E. Holland, EUV spectra of highly-charged ions W^{54+} - W^{63+} relevant to ITER diagnostics, *J Phys B: At , Mol Opt Phys* 41 (2) (2008) 021003. doi:10.1088/0953-4075/41/2/021003.
- [15] U. I. Safronova, A. S. Safronova, Wavelengths and transition rates for $nl-n'l'$ transitions in Be-, B-, Mg-, Al-, Ca-, Zn-, Ag- and Yb-like tungsten ions, *J. Phys. B: At., Mol. Opt. Phys.* 43 (7) (2010) 074026. doi:10.1088/0953-4075/43/7/074026.
- [16] P. Quinet, Dirac-Fock calculations of forbidden transitions within the $3p^k$ and $3d^k$ ground configurations of highly charged tungsten ions (W^{47+} - W^{61+}), *J. Phys. B: At., Mol. Opt. Phys.* 44 (19) (2011) 195007. doi:10.1088/0953-4075/44/19/195007.

- [17] Y. Ralchenko, I. N. Draganić, D. Osin, J. D. Gillaspy, J. Reader, Spectroscopy of diagnostically important magnetic-dipole lines in highly charged $3d^n$ ions of tungsten, *Phys. Rev. A* 83 (2011) 032517. doi:10.1103/PhysRevA.83.032517.
- [18] C. F. Fischer, G. Gaigalas, P. Jonsson, Core effects on transition energies for $3d^k$ configurations in tungsten ions, *Atoms* 5 (01) (2017) 010007. doi:10.3390/atoms5010007.
- [19] X. Ding, S. Rui, K. Fumihiko, D. Kato, I. Murakami, H. A. Sakaue, C. Dong, Correlation, Breit and Quantum Electrodynamics effects on energy level and transition properties of W^{54+} ion, *Eur. Phys. J. D* 71 (2017) 73. doi:10.1140/epjd/e2017-70829-y.
- [20] X. Ding, S. Rui, K. Fumihiko, I. Murakami, D. Kato, H. A. Sakaue, N. Nakamura, C. Dong, Energy levels, lifetimes and radiative data of W LV, *At. Data Nucl. Data Tables* (2017)(In Press). doi:10.1016/j.adt.2017.02.002.
- [21] K. Slabkowska, J. Rzadkiewicz, . Syrocki, E. Szymaska, A. Shumack, M. Polasik, N. R. Pereira, J. contributors, On the interpretation of high-resolution x-ray spectra from JET with an ITER-like wall, *J. Phys. B: At., Mol. Opt. Phys.* 48 (14) (2015) 144028. doi:10.1088/0953-4075/48/14/144029.
- [22] X. Ding, I. Murakami, D. Kato, H. A. Sakaue, F. Koike, C. Dong, Collisional-radiative modeling of W^{27+} , *Plasma Fusion Res.* 7 (2012) 2403128–2403128. doi:10.1585/pfr.7.2403128.
- [23] M. L. Qiu, R. F. Zhao, X. L. Guo, Z. Z. Zhao, W. X. Li, S. Y. Du, J. Xiao, K. Yao, C. Y. Chen, R. Hutton, Y. Zou, Investigation of transitions between metastable levels of the first excited configuration of palladium-like tungsten, *J. Phys. B: At., Mol. Opt. Phys.* 47 (17) (2014) 175002. doi:10.1088/0953-4075/47/17/175002.
- [24] X. Ding, J. Liu, F. Koike, I. Murakami, D. Kato, H. A. Sakaue, N. Nakamura, C. Dong, Collisional-radiative model for the visible spectrum of W^{26+} ions, *Phys. Lett. A* 380 (7-8) (2016) 874–877. doi:10.1016/j.physleta.2015.12.034.
- [25] M. L. Qiu, W. X. Li, Z. Z. Zhao, Y. Yang, J. Xiao, T. Brage, R. Hutton, Y. Zou, Review of highly charged tungsten spectroscopy research using low energy EBITs at the Shanghai EBIT laboratory, *J. Phys. B: At., Mol. Opt. Phys.* 48 (14) (2015) 144029. doi:10.1088/0953-4075/48/14/144029.
- [26] M. F. Gu, The flexible atomic code, *Can. J. Phys.* 730 (5) (2008) 127–136. doi:10.1139/P07-197.
- [27] Y. Ralchenko, I. N. Draganić, D. Osin, J. D. Gillaspy, J. Reader NIST ASD Team. NIST Atomic Spectra Database (ver. 5.2),online at <http://physics.nist.gov/asd>, 2011.